The Journal of Chemical Physics PERSPECTIVE scitation.org/journal/jcp

Field theoretic approach for block polymer melts: SCFT and FTS

Cite as: J. Chem. Phys. 152, 110901 (2020); doi: 10.1063/1.5145098
Submitted: 14 January 2020 • Accepted: 20 February 2020 •
Published Online: 16 March 2020

M. W. Matsen[a)]

AFFILIATIONS

Department of Chemical Engineering, Department of Physics and Astronomy, and Waterloo Institute for Nanotechnology, University of Waterloo, Waterloo, Ontario N2L 3G1, Canada

[a)]Author to whom correspondence should be addressed: mwmatsen@uwaterloo.ca

ABSTRACT

This perspective addresses the development of polymer field theory for predicting the equilibrium phase behavior of block polymer melts. The approach is tailored to the high-molecular-weight limit, where universality reduces all systems to the standard Gaussian chain model, an incompressible melt of elastic threads interacting by contact forces. Using mathematical identities, this particle-based version of the model is converted to an equivalent field-based version that depends on fields rather than particle coordinates. The statistical mechanics of the field-based model is typically solved using the saddle-point approximation of self-consistent field theory (SCFT), which equates to mean field theory, but it can also be evaluated using field theoretic simulations (FTS). While SCFT has matured into one of the most successful theories in soft condensed matter, FTS are still in its infancy. The two main obstacles of FTS are the high computational cost and the occurrence of an ultraviolet divergence, but fortunately there has been recent groundbreaking progress on both fronts. As such, FTS are now well poised to become the method of choice for predicting fluctuation corrections to mean field theory.

I. INTRODUCTION

Block polymers refer to polymer molecules involving two or more sections (i.e., blocks) formed from chemically distinct monomers.[1] The general incompatibility of the unlike blocks tempered by their connectivity causes these macromolecules to self-assemble into periodically ordered morphologies. The wide range of polymeric architectures (e.g., linear, star, and comb) and the potential for blending different molecules lead to an endless array of systems.[2–5] The applications are so numerous and diverse,[5,6] with new ones continuously emerging, that we do not attempt to describe them here. Instead, we focus on efforts to predict their equilibrium phase behavior using polymer field theory.

In order to best illustrate the approach, we consider the simplest system, a neat melt of linear diblock polymers, each composed of N_A A-type segments joined to N_B B-type segments. We follow the convention where monomers are grouped together into larger coarse-grained segments of a given volume, ρ_0^{-1}. Rather than specifying N_A and N_B, a diblock is usually characterized by its total number of segments, $N \equiv N_A + N_B$, and its composition, $f \equiv N_A/N$. In general, the A and B segments will possess different statistical lengths, a_A and a_B, respectively, from which one defines the average segment length, $a \equiv \sqrt{fa_A^2 + (1-f)a_B^2}$.

In a melt, the typical size of an entire molecule is given by its radius of gyration, $R_g = a\sqrt{N/6}$. Assuming N is large, there will, therefore, exist a clear separation between the atomistic and molecular length scales, a and R_g, respectively. Consequently, the complicated atomistic structure of the monomers becomes irrelevant on the molecular scale, and in turn, the equilibrium phase behavior becomes universal on the molecular (or coarse-grained) scale.[7,8] Although this universality has been evident in experiments from early on,[9] not until recently was it shown to be precise.[10–13] The profound implication is that simple models can provide quantitatively accurate predictions.[14]

The Gaussian chain model (GCM) has emerged as the standard model for block polymer phase behavior.[15] It is a minimal model that only contains the essential features, whereby a melt is treated as an incompressible system of elastic threads interacting by contact forces. The strength of the interactions is controlled by the usual Flory–Huggins χ parameter. In polymer field theory, this particle-based Hamiltonian is converted to a field-based

Hamiltonian, $H[W_-, W_+]$, which depends on a composition field, $W_-(\mathbf{r})$, coupling to the difference in A and B concentration and a pressure field, $W_+(\mathbf{r})$, enforcing the incompressibility.

Self-consistent field theory (SCFT)[16] approximates the fields by the saddle point of $H[W_-, W_+]$, which corresponds to the mean field approximation. The first application of SCFT to diblock polymers was by Helfand in 1975,[17] but it initially received limited attention in favor of analytical theories because of the computational challenges of applying it beyond 1D problems (i.e., the lamellar phase). In 1980, Leibler[18] developed a random-phase approximation (RPA) which provided a phase diagram for the classical lamellar (L), cylindrical (C), and spherical (S) phases at weak segregations, $\chi N \sim 10$. Then, in 1985, Semenov[19] developed a strong-segregation theory (SST) which provided the phase boundaries in the limit of $\chi N \to \infty$. Helfand and Wasserman[20] did eventually estimate the SCFT phase diagram by invoking a sharp interface approximation combined with a unit-cell approximation that reduces the C and S phases to 1D problems. The assumption of sharp interfaces was later removed by Vavasour and Whitmore,[21] providing a phase diagram of the classical phases that bridged between the RPA and SST limits.

Following the successful treatment of the classical phases, block polymer research experienced a period of intense activity as experimentalists began to observe complex phases situated between the L and C regions. These included the double-diamond (D),[22] gyroid (G),[23,24] perforated-lamellar (PL),[25] and modulated-lamellar (ML)[25] phases. Efforts were made to extend the RPA and SST beyond the classical phases, but SCFT soon gained the upper hand with the introduction of a spectral algorithm that allowed numerical calculations free of approximation.[26] Figure 1 shows the resulting phase diagram. The SCFT predicted G to be stable, PL to be highly metastable, D to be far from stable, and ML to be unstable. At first, these findings seemed to contradict experiment, but they would ultimately prove to be correct. The first revelation occurred when samples initially identified as D turned out to be G under re-examination;[27] there now remains no credible evidence that D ever occurred in neat diblock polymer melts. The next revelation was that PL eventually converts to G if annealed for sufficient time,[28,29] confirming the prediction that PL is metastable; it is now understood that the intermediate PL phase forms due to a low-energy kinetic pathway from the L phase.[30] The evidence for ML has since been attributed to nothing more than fluctuations in the simple L phase,[31] such as transient perforations.[32] The latest addition to the complex phase window was the Fddd (O^{70}) phase, initially predicted by Tyler and Morse.[33] Within two years of the prediction, experiments identified it in PS–PI diblocks on the PS-rich side of the phase diagram[34] and then later on the PI-rich side.[35]

With the complex phase window resolved, attention switched to the spherical region.[36] The usual arrangement of spherical domains is bcc, as first predicted by RPA.[18] SST also predicts narrow regions of closed-packed (fcc or hcp) spheres along the order-disorder transition (ODT).[37] Although SCFT finds that hcp is slightly favored over fcc,[38] the energy difference is too small to produce long-range order,[39] as evident by the fact that experiments observe a disordered array of close-packed spheres.[40,41] The renewed interest in the spherical region began in 2010, when Lee *et al.*[42] discovered the Frank–Kasper sigma (σ) phase, involving a large tetragonal unit cell containing 30 spherical domains. SCFT calculations by

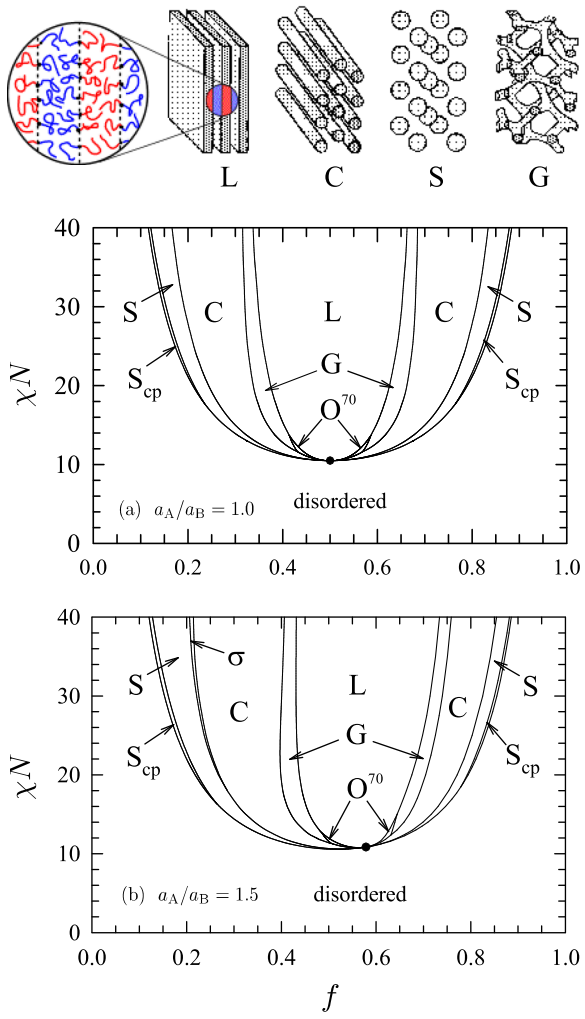

FIG. 1. SCFT phase diagrams for diblock polymer melts with conformationally (a) symmetric and (b) asymmetric segment lengths, a_A and a_B, plotted in terms of the Flory–Huggins χ parameter, the degree of polymerization, N, and the composition, f. The labels denote the ordered lamellar (L), cylindrical (C), bcc spherical (S), hcp spherical (S_{cp}), gyroid (G), Fddd (O^{70}), and sigma (σ) phases. The schematic images at the top illustrate the geometry of the A- and B-rich domains within the L, C, S, and G phases.

Xie *et al.*[43] predicted the σ phase to occur if a_A/a_B deviated sufficiently from one, and shortly after, experiments[44] confirmed the stabilizing effect of conformational asymmetry. The experiments, however, found that the σ phase requires less conformational asymmetry than predicted by SCFT. They have attributed this to fluctuation effects omitted by SCFT,[45] while SCFT calculations suggest that it results from polydispersity effects.[46] At even higher conformational asymmetry, another spherical phase, A15, emerges between the σ and C regions.[47] As with the σ phase, A15 occurs at a lower asymmetry in experiments than predicted by SCFT. Again fluctuations and polydispersity are potential explanations for its enhanced stability.

Despite its remarkable track record regarding ordered phases, SCFT treats the disordered phase very inaccurately.[11,48] In particular, it predicts uniform mixing of the A and B segments, which contradicts the strong scattering observed in experiments.[49] In 1987, Fredrickson and Helfand[50] evaluated the effect of composition fluctuations on the SCFT phase diagram. For symmetric diblocks (i.e., $f = 0.5$ and $a_A = a_B$), they predicted an ODT of

$$(\chi N)_{\mathrm{ODT}} = 10.495 + 41.0\bar{N}^{-1/3}, \tag{1}$$

where the size of the fluctuation correction is controlled by the invariant polymerization index, $\bar{N} \equiv a^6\rho_0^2 N$. A somewhat more refined calculation by Mayes and de la Cruz[51] gives a coefficient of 39.0 for the correction instead of 41.0. In any case, the approximations involved are only accurate for $\bar{N} \gtrsim 10^{10}$, which far exceeds the typical range, $10^2 \lesssim \bar{N} \lesssim 10^4$, of experiments.[9]

Field theoretic simulations (FTS) offer a way of obtaining accurate fluctuation corrections to SCFT, by simulating the Hamiltonian, $H[W_-, W_+]$. However, standard simulation techniques for integrating over the fields are not applicable. Although the composition field, $W_-(\mathbf{r})$, takes on real values, the pressure field, $W_+(\mathbf{r})$, is imaginary, which leads to a complex-valued Hamiltonian, and thus, a Boltzmann weight that is not positive definite. Ganesan and Fredrickson[52] dealt with this using two different strategies. The first was a steepest descent technique (STD-FTS), which shifts the integration so that it follows a constant-phase path through the saddle points of SCFT, and the second was complex Langevin simulations (CL-FTS), whereby both fields sample the entire complex plane. The later method was deemed to be more efficient.

In 2008, Lennon *et al.*[53] used the CL-FTS to elevate fluctuation corrections to the ODT of diblock polymer melts. The simulations, however, were limited to an invariant polymerization index of $\bar{N} = 5.4 \times 10^5$, which far exceeds the typical values of experiments. They were unable to consider smaller $\bar{N}$ because of an instability that causes the fields to diverge.[54,55] Delaney and Fredrickson[56] have since managed to tame the instability by introducing compressibility and smearing the interactions, allowing them to generate a phase diagram for $\bar{N} \approx 10^4$.

Another strategy is to perform a partial saddle-point approximation, where $W_-(\mathbf{r})$ fluctuates, while the pressure field follows its saddle point, $w_+(\mathbf{r})$, which turns out to be real. Consequently, the resulting Hamiltonian, $H[W_-, w_+]$, is also real, which then allows for standard simulation techniques. Comparisons with CL-FTS have shown the approximation to be relatively accurate.[57,58] The first implementation of the partial saddle-point approximation used ordinary Langevin simulations (L-FTS),[59] but this work was largely overlooked and Monte Carlo simulations (MC-FTS) prevailed.[57,60–67] Only recently was it realized that L-FTS are actually far superior to MC-FTS.[68] An important advantage of the partial saddle-point approximation is that it removes the instability, allowing for simulations at lower $\bar{N}$.[62,63,68]

In FTS, the fields are generally represented on a discrete grid with some finite spacing, Δ. One might expect the results to become increasingly accurate as $\Delta \to 0$, but this is subverted by an ultraviolet (UV) divergence. De la Cruz *et al.*[69] were the first to investigate the divergence and argued that it could be removed by renormalizing the χ parameter. Stasiak and Matsen[61] demonstrated that the renormalization works well for large $\bar{N}$, but Vorselaars and Matsen[62] later found that it starts to fail just as the experimentally relevant regime is approached. They proposed an alternative renormalization that seemed to work when applied to diblock polymer melts, but it failed for homopolymer melts.[64] Nevertheless, Beardsley and Matsen[63] have now resolved the issue by instead defining χ according to the Morse calibration procedure devised for particle-based simulations.[70] The UV divergence can also be removed by modifying the model, which is, in fact, what Delaney and Fredrickson[56] did when they included compressibility and smeared the interactions. However, doing so requires mapping the parameters of the modified model back onto those of the standard GCM, which could likewise be accomplished with the Morse calibration.

There are numerous reviews on SCFT[15,39,71,72] as well as a few on FTS,[73–75] which we do not attempt to repeat. Now that FTS have proven to be a practical alternative to traditional particle-based simulations, we can expect to see a substantial uptake in its application. To help facilitate this, the present perspective is aimed at those, which may have experience in SCFT but are otherwise new to FTS. It provides an overarching description of the field theoretic approach, reviews the current state-of-the-art in numerical methods, discusses outstanding problems, and assesses the future outlook. So as to provide the most transparent discussion possible, we concentrate on neat diblock polymer melts. Nevertheless, one of the main advantages of the field theoretic approach is its incredible versatility, and so some discussion on its extension to more complex systems is included.

II. STANDARD GAUSSIAN CHAIN MODEL

This section describes the standard GCM for a melt of n diblock polymers, each consisting of N coarse-grained segments of volume ρ_0^{-1}. As illustrated in Fig. 2, the polymer configurations are specified by the space curves $\mathbf{r}_\alpha(t)$, where the molecule index $\alpha = 1, 2, \ldots, n$ and the contour variable takes on values $t \in (0, fN)$ along the A block and $t \in (fN, N)$ along the B block. The individual segments are themselves polymer coils, and thus, they can stretch. However, they lose entropy as they do so, the cost of which increases as the square of

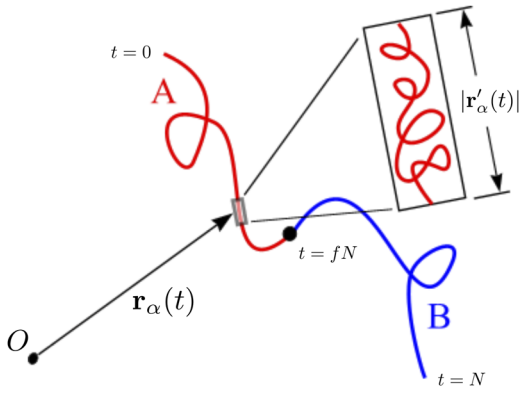

FIG. 2. Space curve, $\mathbf{r}_\alpha(t)$, specifying the coarse-grained configuration of a diblock polymer. The molecular index takes on values $\alpha \in \{1, 2, 3, \ldots, n\}$, and the contour variable takes on values $t \in (0, fN)$ along the A block and $t \in (fN, N)$ along the B block. The individual segments are polymer coils on the atomistic scale, and thus, they can stretch.

their end-to-end length, a direct consequence of the central limit theorem from statistics. As a result, the polymers behave as ideal elastic threads, which is handled by weighting each configuration $\mathbf{r}_\alpha(t)$ by the probability,

$$P_\alpha = \exp\left(-\frac{3}{2}\int_0^N \frac{|\mathbf{r}'_\alpha(t)|^2}{\beta(t)}dt\right). \tag{2}$$

The conformational asymmetry between the statistical lengths a_A and a_B of the A and B segments, respectively, is accounted for by the function,

$$\beta(t) = \begin{cases} a_A^2 & \text{for } t < fN \\ a_B^2 & \text{for } t > fN. \end{cases} \tag{3}$$

Given the space curves, we can conveniently express the concentration of A segments as

$$\hat{\phi}_A(\mathbf{r}) = \frac{1}{\rho_0}\sum_{\alpha=1}^{n}\int_0^{fN}\delta(\mathbf{r}-\mathbf{r}_\alpha(t))dt. \tag{4}$$

Similarly, the concentration of B segments, $\hat{\phi}_B(\mathbf{r})$, is given by an analogous expression, where the integration instead extends over $t \in (fN, N)$.

To complete the model, one needs to include molecular interactions. For a microscopic model, one might choose Lennard-Jones interactions, but this is inappropriate for a coarse-grained model. Nevertheless, the same physics must be included. The hard-core part of the interactions is responsible for a relatively uniform density, and therefore, the standard GCM accounts for this by enforcing the incompressibility constraint $\hat{\phi}_A(\mathbf{r}) + \hat{\phi}_B(\mathbf{r}) = 1$. The attractive part of the interactions is longer range but still short range compared to R_g, and therefore, it is treated by pairwise contact forces. As a result of incompressibility, there is no need to include interactions between segments of the same type, and thus, the internal energy is expressed as

$$\frac{U}{k_BT} = \rho_0\chi_b\int \hat{\phi}_A\hat{\phi}_B d\mathbf{r}, \tag{5}$$

where the Flory–Huggins χ_b parameter controls the "bare" strength of the A–B interactions.

It is important to appreciate that the five model parameters, χ, N, f, a_A, and a_B, are not uniquely defined. This is because of the freedom one has to redefine the coarse-grained segments by changing ρ_0. If one increases ρ_0 by a factor of λ, then χ will decrease by a factor λ, N will increase by a factor λ, and the two segment lengths will both decrease by a factor of $\sqrt{\lambda}$. There are, in fact, only four independent quantities, $\chi N, f, a_A/a_B$, and $\bar{N}$, which remain invariant with respect to changes in ρ_0, and it is their values that control the phase behavior.

We are interested in studying the equilibrium behavior of the standard GCM using statistical mechanics, which requires the evaluation of the partition function,

$$Z \propto \int \exp\left(-\frac{U}{k_BT}\right)\delta[\hat{\phi}_A + \hat{\phi}_B - 1]\prod_{\alpha=1}^{n} P_\alpha \mathcal{D}\mathbf{r}_\alpha. \tag{6}$$

The integrand of Z includes a Boltzmann weight for the interactions, a Dirac delta functional to enforce incompressibility, and a weighting function, P_α, for the entropic stretching energy of each polymer. The functional integration is then performed over the configurations, $\mathbf{r}_\alpha(t)$, of all n polymers. Before addressing how to evaluate Z, we first discuss the validity of the standard GCM and how to relate it to experiments.

III. UNIVERSALITY

The significance of universality is that virtually any model can be calibrated to provide quantitative predictions for any particular experiment. To avoid the need to recalibrate each model for every different experimental system, it is best to calibrate all systems with respect to a reference model. Naturally, it is best to select a "minimal" model, which contains only the essential features of the block polymer melt and thus involves the least number of parameters possible. The standard GCM nicely serves this purpose.

The universality of block polymer melts has been evident from early on. This was well illustrated by Bates *et al.*,[9] when they showed that the phase diagrams of four chemically distinct diblock systems were remarkably similar when plotted in terms of χN and f.[9] The minor differences could be attributed to variations in a_A/a_B and $\bar{N}$. However, the equivalence was not initially regarded as exact, but evidence is now mounting that the universality is, in fact, quantitative.[8,10–13] In particular, different simulation models for symmetric diblock polymer melts are found to exhibit a universal ODT given by[10–12]

$$(\chi N)_{\mathrm{ODT}} = 10.495 + 41.0\bar{N}^{-1/3} + 123.0\bar{N}^{-0.56}, \tag{7}$$

where the third term is an empirical correction to the Fredrickson–Helfand prediction in Eq. (1). There is also compelling evidence that the equivalence extends to experiments.[14] In reality, this follows logically from the fact that models can be extended to provide arbitrarily accurate representations of real experiments.

The universality hypothesis implies that the parameters of any experiment (or simulation) can be mapped onto those of the standard GCM. The mappings of N and f are trivial given their straightforward definitions in terms of molecular volume. The statistical segment lengths are also readily defined by the fact that the radius of gyration of linear homopolymers in a neat melt is given by $R_g = a\sqrt{N/6}$ for large N. The only non-trivial aspect of the mapping is how to define the Flory–Huggins χ parameter.

The determination of χ has been a longstanding problem to which numerous strategies have been applied.[76–87] Unfortunately, the different methods result in different values of χ, leading many to conclude that χ depends on composition, architecture, molecular weight, polydispersity, or basically all the parameters of the system. Others come to the conclusion that χ has no clearcut definition. The problem stems from the way χ is determined, which always involves measuring some quantity by experiment (or simulation) and then fitting to a prediction of the standard GCM. For χ to be accurate, not only does the measurement need to be accurate but so does the prediction. In most cases, the prediction is based on mean field theory, which, in effect, buries fluctuation corrections into the χ parameter. Thus, it should be of no surprise that the parameters derived from different quantities are themselves different, since they possess distinct fluctuation corrections. Furthermore, fluctuation effects depend on all the parameters of the system, and thus, the resulting χ will also depend on all the parameters.

Morse and co-workers have made great progress in resolving the issue of how to define χ. For weak interactions, it is uniquely defined by the requirement that mean field theory becomes exact in the $\bar{N} \to \infty$ limit. However, the definition of χ at stronger interactions requires choosing a quantity to fit. Naturally, it should be one that we can predict accurately. Glaser and co-workers[8] selected the disordered-state structure function, $S(k)$, for symmetric diblock polymer melts, as predicted by renormalized one-loop (ROL) calculations, arguably the most accurate prediction available. It is this choice that was used to demonstrate the universality among the different simulation models[10–13] and between experiment and simulation.[14]

IV. FIELD THEORETIC MODEL

Even though the partition function in Eq. (6) looks simple, the functional integrals cannot be evaluated directly due to the complicated dependence of $\exp(-U/k_BT)$ and $\delta[\hat{\phi}_A+\hat{\phi}_B-1]$ on the polymer configurations, $\mathbf{r}_\alpha(t)$. This problem can, however, be dealt with by switching from a particle- to a field-based model,[74] as illustrated in Fig. 3. To start, the incompressibility constraint is used to re-express the interaction energy, to within an additive constant, as

$$\frac{U}{k_BT} = \frac{\rho_0\chi_b}{4}\int(\hat{\phi}_A-\hat{\phi}_B)^2 d\mathbf{r}, \tag{8}$$

where $\hat{\phi}_A(\mathbf{r})-\hat{\phi}_B(\mathbf{r})$ is the composition of the melt. The Hubbard–Stratonovich identity,

$$e^{\alpha u^2} = \frac{1}{\sqrt{\pi\alpha}}\int_{-\infty}^{\infty} e^{-\left(\frac{v^2}{\alpha}+2vu\right)}dv, \tag{9}$$

is then applied at each point in space, $\mathbf{r}$, with u set to the composition and v set to a "composition" field, $W_-(\mathbf{r})$. This results in the relationship

$$\exp\left(-\frac{U}{k_BT}\right) \propto \int \exp\left(-\frac{n}{V}\int\left[\frac{W_-^2}{\chi_b}-W_-(\hat{\phi}_A-\hat{\phi}_B)\right]d\mathbf{r}\right)\mathcal{D}W_-, \tag{10}$$

where the polymer concentrations couple linearly to the field. Similarly, the Fourier representation of the Dirac delta function,

$$\delta(u) = \frac{1}{2\pi}\int_{-i\infty}^{i\infty} e^{vu}dv, \tag{11}$$

is applied at each point in space, $\mathbf{r}$, this time setting u to the deviation from incompressibility and v to a "pressure" field, $W_+(\mathbf{r})$. This leads to the mathematical identity

$$\delta[\hat{\phi}_A+\hat{\phi}_B-1] \propto \int \exp\left(-\frac{n}{V}\int W_+(\hat{\phi}_A+\hat{\phi}_B-1)d\mathbf{r}\right)\mathcal{D}W_+, \tag{12}$$

where the polymer concentrations again couple linearly to the field.

Inserting Eqs. (10) and (12) into Eq. (6) for Z allows the functional integrations over $\mathbf{r}_\alpha(t)$ to be performed analytically due to the linear dependence on concentration. The partition function is then recast in the form

$$Z \propto \int \exp\left(-\frac{H[W_-,W_+]}{k_BT}\right)\mathcal{D}W_-\mathcal{D}W_+, \tag{13}$$

where

$$H = H_Q + k_BT\rho_0\int\left(\frac{W_-^2}{\chi_b}-W_+\right)d\mathbf{r} \tag{14}$$

defines a field-based Hamiltonian.[73,75] It involves the Hamiltonian,

$$H_Q = -nk_BT\ln Q, \tag{15}$$

for a system of n noninteracting polymers in the canonical ensemble, which is expressed in terms of the single-chain partition function,

$$Q \propto \int \exp\left(-\int[W_+(\mathbf{r}_\alpha)+\gamma W_-(\mathbf{r}_\alpha)]dt\right)P_\alpha\mathcal{D}\mathbf{r}_\alpha, \tag{16}$$

where

$$\gamma(t) = \begin{cases} 1 & \text{for } t < fN \\ -1 & \text{for } t > fN \end{cases} \tag{17}$$

distinguishes between the A and B blocks.

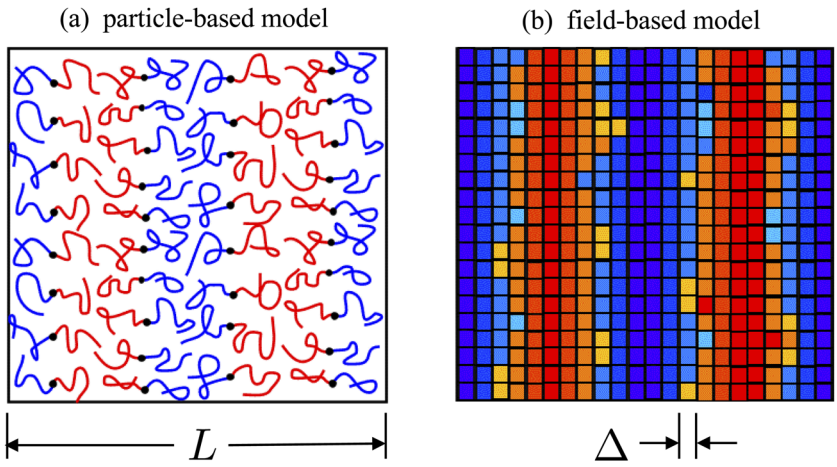

FIG. 3. Comparison of (a) the particle-based model corresponding to Eq. (6), where the configuration of the system is specified by $\mathbf{r}_\alpha(t)$, and (b) the field-based model corresponding to Eq. (13), where the configuration is specified by $W_-(\mathbf{r})$ and $W_+(\mathbf{r})$.

Both SCFT and FTS will require the functional derivatives of $H[W_-, W_+]$ with respect to each of its fields. The first is given by

$$\frac{1}{k_BT\rho_0}\frac{\mathcal{D}H}{\mathcal{D}W_-} = \phi_-(\mathbf{r}) + \frac{2}{\chi_b}W_-(\mathbf{r}), \tag{18}$$

where

$$\phi_-(\mathbf{r}) = -\frac{V}{NQ}\frac{\mathcal{D}Q}{\mathcal{D}W_-} \tag{19}$$

is the composition of n non-interacting diblocks in the fields. Similarly, the second is given by

$$\frac{1}{k_BT\rho_0}\frac{\mathcal{D}H}{\mathcal{D}W_+} = \phi_+(\mathbf{r}) - 1, \tag{20}$$

where

$$\phi_+(\mathbf{r}) = -\frac{V}{NQ}\frac{\mathcal{D}Q}{\mathcal{D}W_+} \tag{21}$$

is the total concentration of n non-interacting diblocks in the fields.

V. POLYMER IN A FIELD

The transformation to a field-based model effectively reduces the statistical mechanics of the system to that of a single molecule in the fields $W_-(\mathbf{r})$ and $W_+(\mathbf{r})$. Its partition function is conveniently expressed as

$$Q = \frac{1}{V}\int q(\mathbf{r},t)q^\dagger(\mathbf{r},t)d\mathbf{r}, \tag{22}$$

where $q(\mathbf{r}, t)$ and $q^\dagger(\mathbf{r}, t)$ are partial partition functions for the $(0, t)$ and (t, N) portions of the chain, respectively, with segment t constrained at position $\mathbf{r}$. Thus, the product $q(\mathbf{r}, t)q^\dagger(\mathbf{r}, t)$ gives the partition function of the entire molecule with segment t fixed at $\mathbf{r}$. The constraint is then removed by integrating over $\mathbf{r}$, providing the partition function of an unconstrained molecule, $Q[W_-, W_+]$.

The reason for introducing the partial partition functions is that they can be readily obtained by solving a modified diffusion equation.[17,88] In particular, $q(\mathbf{r}, t)$ satisfies

$$\frac{\partial q}{\partial t} = \frac{\beta}{6}\nabla^2 q - (W_+ + \gamma W_-)q, \tag{23}$$

and the initial condition $q(\mathbf{r}, 0) = 1$, while $q^\dagger(\mathbf{r}, t)$ satisfies the same equation with one side multiplied by -1 and the condition $q^\dagger(\mathbf{r}, N) = 1$. Applying the functional derivatives in Eqs. (19) and (21) to the definition in Eq. (22) gives

$$\phi_-(\mathbf{r}) = \frac{1}{NQ}\int_0^N \gamma(t)q(\mathbf{r},t)q^\dagger(\mathbf{r},t)dt, \tag{24}$$

$$\phi_+(\mathbf{r}) = \frac{1}{NQ}\int_0^N q(\mathbf{r},t)q^\dagger(\mathbf{r},t)dt. \tag{25}$$

VI. SELF-CONSISTENT FIELD THEORY

Despite the transformation to a field-based Hamiltonian, the functional integrals in Eq. (13) still cannot be performed analytically. However, the partition function of the system can be estimated by

$$Z \propto \exp\left(-\frac{H[w_-, w_+]}{k_BT}\right), \tag{26}$$

where $w_-(\mathbf{r})$ and $w_+(\mathbf{r})$ denote the saddle point of $H[W_-, W_+]$. Referring to Eqs. (18) and (20), it follows that

$$w_-(\mathbf{r}) = -\frac{\chi}{2}\phi_-(\mathbf{r}), \tag{27}$$

$$\phi_+(\mathbf{r}) = 1. \tag{28}$$

This saddle-point approximation equates to mean field theory, where Eqs. (27) and (28) represent the self-consistent field conditions.

Each phase of a block polymer melt corresponds to a distinct locally stable solution of the field equations. The solutions are generally located iteratively, starting from initial guesses, which can be generated from *a priori* knowledge of the geometry of the composition profile, $\phi_-(\mathbf{r})$. In the case of periodic phases, the dimensions of the unit cell have to be adjusted so as to minimize the free energy, $F = H[w_-, w_+]$. Once the solutions for the candidate phases have been obtained, the one with the lowest free energy is assumed to be the stable phase, while the remaining ones correspond to metastable phases. The main limitation of this SCFT procedure is that it does not predict the candidate phases but rather requires them as an input, provided usually by experiments. Even though SCFT showed Fddd to be stable prior to its experimental observation in diblock polymer melts, the phase was, nevertheless, discovered by experiments on ABC triblock polymer melts.[89] The obvious problem is that the global minimum might not be included among the candidate phases, and therefore, we cannot be absolutely certain that all the equilibrium phases are accounted for in phase diagrams like those in Fig. 1.

Efforts to address this shortcoming began with the screening method proposed by Drolet *et al.*,[90] where candidate structures are generated by solving the field equations in real-space starting from randomly generated fields. There have been proposed improvements, whereby the diffusion equation is instead solved using pseudospectral[91] or spectral[92] algorithms. Bohbot-Raviv and Wang[93] proposed using a weak-segregation approximation to SCFT to help increase the computational speed of the search. Xu *et al.*[94] have also tried to improve the search by incorporating existing knowledge into the initialization of the fields. The latest innovation has been the use of genetic algorithms.[95] While these approaches have found new morphologies in ABC triblock polymer melts, this in itself is not much of a test given the zoo of existing phases.[3] It still remains uncertain how effective these searches actually are, but nevertheless, they address an important problem worthy of further effort. Another valuable and perhaps more challenging endeavor is the inverse problem of specifying a desired morphology and trying to find the system parameters for which it is stable. This problem has recently been tackled using particle swarm optimization.[96,97]

Although the standard GCM omits atomistic details, it is still a microscopic model. Thus, SCFT is able to provide a wealth of information, such as the distribution of various segments, details regarding the polymer configurations, and different contributions to the free energy.[98,99] It can also be used to investigate the stability

of ordered phases, the calculation of which closely follows band-structure calculations for crystalline solids;[100–103] a valuable byproduct of that calculation is the scattering function for ordered phases.[31] There is also an innovative "string" method for locating transition pathways between different ordered phases.[30]

VII. RELATED THEORIES

There are a couple analytical theories for the standard GCM, which nicely compliment the numerical SCFT. One is the strong-segregation theory (SST) of Semenov,[19] corresponding to $\chi N \to \infty$. In this limit, diblock morphologies decompose into opposing brushes of A- and B-type chains separated by internal interfaces. The SST assumes the chains are so strongly stretched that they remain in ground-state configurations, referred to as classical paths due to an analogy with classical mechanics.[104] The original application to diblock melts was limited to the L, C, and S phases because it applied the unit-cell approximation for which the classical paths adopt straight trajectories normal to the interfaces. With the discovery of the complex phases, researchers tried to generalize the SST. Olmsted and Milner[105–107] and Likhtman and Semenov[108] extended it to complex phases but required assumptions regarding the shape of the interfaces. Likhtman and Semenov[109] later introduced a version of SST in which the interfacial shape is determined through minimization of the free energy. Although it still assumes straight trajectories and ignores so-called exclusion zones, it does provide the best evidence to date that the G phase in Fig. 1(a) does not extend to infinite segregation,[38] contrary to speculations based on SCFT calculations.[110]

Although the SST makes a few reasonably accurate predictions, such as the position of order–order transitions and the periodicity of the ordered phases,[39] careful quantitative comparisons with SCFT have indicated that it may not represent the true strong-segregation limit.[111] Likhtman and Semenov[112] addressed this issue by analyzing the dominant corrections to SST, which included a correction to the interfacial tension and fluctuations about the classical paths.[113] These corrections bring SST into good qualitative agreement with SCFT, and eventually quantitative agreement, although only at extremely high segregations of $\chi N \gtrsim 10^6$.[114]

Despite its quantitative limitations, SST has been instrumental in developing an intuitive explanation of block polymer phase behavior in terms of a competition between the interfacial energy and the stretching energy of the opposing brushes.[19,115] First, the domain size is determined by balancing the stretching energy, which prefers small domains, against the interfacial energy, which prefers large domains. Second, the competition between the stretching energies of the opposing brushes imparts a spontaneous curvature to the interface, favoring the shorter blocks on the inside of curvature. Consequently, the lamellar phase occurs at symmetric compositions (i.e., $f \approx 0.5$) with the complex phases, then cylinders, and finally spheres as the diblocks become increasingly asymmetric. The selection among the different complex phases is controlled by a subtler effect, packing frustration.[116] The stretching energy favors domains of uniform thickness, while interfacial tension favors interfaces of constant mean curvature. Packing frustration refers to the inability of a morphology to simultaneously satisfy both tendencies. The preference for the G phase is simply a result of low packing frustration. Likewise, packing frustration plays a key role in selecting among the different spherical phases (e.g., bcc, fcc, hcp, σ, and A15).

In the opposite limit, Leibler[18] developed a weak-segregation approximation to SCFT, where the random-phase approximation (RPA) is used to expand the free energy, F, to fourth-order in the composition, $\phi_-(\mathbf{r})$. The calculation is well-known for predicting a critical point in the diblock phase diagram [e.g., the dot in Fig. 1(a) at $(\chi N)_{\mathrm{ODT}} = 10.495$] and the topology of the phase boundaries emerging from the critical point. A useful byproduct of the expansion is a simple analytical expression for the disordered-state structure function, $S(k)$. The initial RPA calculation only included the principle wavevectors of magnitude k^*, which limited it to the classical L, C, and S phases. Podneks and Hamley[117] as well as Milner and Olmsted[118] have since incorporated higher-order wavevectors, so as to account for the G phase. Ranjan and Morse[119] later did the same for the Fddd phase.

The RPA theory also provides the foundation upon which Fredrickson and Helfand[50] calculated fluctuation corrections to the mean field theory and, in particular, the famous expression in Eq. (1) for the ODT of symmetric diblocks. The F–H theory has since been extended by Podneks and Hamley[117] to include the G phase and by Miao and Wickham[120] to include the Fddd phase. While the former calculation predicts direct G-to-disorder transitions, which is consistent with experiments, the later calculation predicts the destruction of the Fddd phase, which is inconsistent with experiments. This is likely due to the inaccuracy of the F–H theory at experimentally relevant values of $\bar{N}$. The F–H theory also improves upon the disordered-state structure function, predicting the peak, $S(k^*)$, to remain finite and its position to shift to smaller k^* as the ODT is approached, which brings the behavior of $S(k)$ into better agreement with experiments.[121] Morse and co-workers[122,123] have improved upon this even further with a renormalized one-loop (ROL) calculation of $S(k)$, which now stands as one of the most accurate predictions for the standard GCM.[8,124] Figure 4 compares the different predictions of $S(k)$ for symmetric diblocks at $\chi N = 8.0$ and $\bar{N} = 500$.

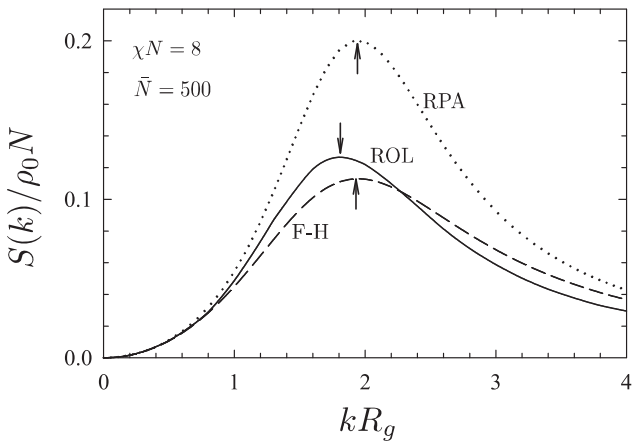

FIG. 4. RPA,[18] F–H,[50] and ROL[123] predictions of the disordered-state structure function, $S(k)$, for $\chi N = 8.0$, $f = 0.5$, $a_A/a_B = 1.0$, and $\bar{N} = 500$. Arrows point to the peak position, k^*, which provides the typical domain size, $2\pi/k^*$, in the disordered phase.

Not surprisingly, the free energy expansion of RPA breaks down beyond the weak-segregation regime. Ohta and Kawasaki[125] remedied this problem by modifying the higher-order terms, allowing for calculations over the full range of segregation. Muthukumar[126] later incorporated fluctuation corrections to the O–K model. As a result of its computational efficiency, the method has seen widespread use over the years. However, quantitative comparisons with SCFT reveal significant quantitative inaccuracies, and in some cases qualitatively incorrect predictions. This shortcoming was recently addressed by Liu *et al.*[127] with the introduction of an optimized phase field model that greatly improves upon the accuracy of the O–K model while still retaining its computational efficiency. Nevertheless, there is no substitute for the full field theory, if accuracy is of concern.

VIII. FIELD THEORETIC SIMULATIONS

Although Z cannot be solved exactly for the field theoretic Hamiltonian, $H[W_-, W_+]$, it is, nevertheless, possible to simulate it. The simulations are typically performed in a cubic simulation box of volume $V = L^3$ with periodic boundaries (see Fig. 3). In order to represent the fields on a computer, a discrete grid is imposed over the simulation box with m points in each direction separated by a uniform spacing of Δ (i.e., $L = m\Delta$).

As implied by Eq. (11), the integration of $W_+(\mathbf{r})$ needs to be performed over the imaginary axis and therefore standard simulation methods are not applicable. Fredrickson and co-workers[52,72,73,75] have dealt with this by performing complex Langevin simulations (CL-FTS), where both fields are permitted to sample the entire complex plane. In particular, the fields evolve according to the Langevin dynamics,

$$\frac{\partial W_-}{\partial \tau} = -\lambda_- \frac{\mathcal{D}H}{\mathcal{D}W_-} + \hat{\eta}_-, \tag{29}$$

$$\frac{\partial W_+}{\partial \tau} = \lambda_+ \frac{\mathcal{D}H}{\mathcal{D}W_+} + i\hat{\eta}_+, \tag{30}$$

where the functional derivatives are given by Eqs. (18) and (20) and the independent functions $\hat{\eta}_\pm(\mathbf{r}, \tau)$ provide real-valued Gaussian noise, satisfying

$$\langle \hat{\eta}_\pm(\mathbf{r}, \tau) \rangle = 0, \tag{31}$$

$$\langle \hat{\eta}_\pm(\mathbf{r}, \tau) \hat{\eta}_\pm(\mathbf{r}', \tau') \rangle = 2\lambda_\pm k_B T \delta(\mathbf{r} - \mathbf{r}') \delta(\tau - \tau'). \tag{32}$$

The parameters $\lambda_\pm$ control the rate at which the fields evolve, which is only relevant when studying actual dynamics. Here, the Langevin equations are just used to generate a sequence of equilibrated configurations (i.e., $\tau = k\Delta\tau$ for $k = 1, 2, 3, \ldots$), and so we set $\lambda_\pm = 1/k_B T \rho_0$ for convenience. The sequence can be generated with the simple Euler time-stepping iteration,

$$W_-(\mathbf{r}; \tau + \Delta\tau) = W_-(\mathbf{r}; \tau) - [\phi_-(\mathbf{r}; \tau) + 2W_-(\mathbf{r}; \tau)/\chi_b]\Delta\tau + \mathcal{N}(0, \sigma), \tag{33}$$

$$W_+(\mathbf{r}; \tau + \Delta\tau) = W_+(\mathbf{r}; \tau) + [\phi_+(\mathbf{r}; \tau) - 1]\Delta\tau + i\mathcal{N}(0, \sigma), \tag{34}$$

where $\mathcal{N}(0, \sigma)$ provides random numbers from a normal distribution with a mean of zero and a variance of

$$\sigma^2 = \frac{2\Delta\tau}{\Delta^3 \rho_0}. \tag{35}$$

Düchs *et al.*[128] discuss a number of improvements to the Euler algorithm that allow for larger step sizes, $\Delta\tau$.

The issue of complex fields can be avoided by making a partial saddle-point approximation, whereby $W_+(\mathbf{r})$ is replaced by its saddle point, $w_+(\mathbf{r})$, which turns out to be real. This reduces the partition function to

$$Z \propto \int \exp\left(-\frac{H[W_-, w_+]}{k_B T}\right) \mathcal{D}W_-, \tag{36}$$

where $w_+(\mathbf{r})$ satisfies the self-consistent condition in Eq. (28), which amounts to enforcing incompressibility in the mean field approximation. The rationale for this is that the fluctuations in $W_-(\mathbf{r})$ are considerably more important than those in $W_+(\mathbf{r})$, and thus, the approximation still captures the majority of the fluctuation corrections to SCFT. Comparisons with CL-FTS have indeed shown the partial saddle-point approximation to be accurate.[57,58] Although there is only one fluctuating field to integrate over, the self-consistent condition for $w_+(\mathbf{r})$ has to be solved every time $W_-(\mathbf{r})$ changes. Nevertheless, one is generally dealing with small changes in $W_-(\mathbf{r})$, and thus, the cost of updating $w_+(\mathbf{r})$ is small. The advantage of real-valued fields is that standard simulation techniques are applicable. The first implementation used ordinary Langevin simulations (L-FTS),[59] where $W_-(\mathbf{r})$ evolves according to Eq. (33), but the more popular choice has been Monte Carlo simulations (MC-FTS),[57,60–67] where small random changes in $W_-(\mathbf{r})$ are accepted or rejected based on the standard Metropolis algorithm. Just recently, however, a direct head-to-head comparison showed L-FTS to be far faster.[68] It is prudent to remember, though, that the efficiency of MC is highly dependent on the choice of trial moves, and so it is still conceivable that MC could become competitive with the use of more sophisticated moves.[129]

IX. ULTRAVIOLET DIVERGENCE

One would naturally expect FTS to become increasingly accurate as the grid spacing, Δ, approaches zero, but this limit is, in fact, ill-defined due to an ultraviolet (UV) divergence. It results from trying to enforce incompressibility on 1D threads that interact by zero-range contact forces.[70] The divergence would likewise occur if one increased the resolution in particle-based simulations of the standard GCM.[130] The underlying problem is that reducing Δ decreases the relative number of intermolecular contacts,[68] which, in turn, reduces the level of segregation. The issue was first recognized by de la Cruz *et al.*,[69] where they showed that the divergence could be compensated for by renormalizing the bare interaction parameter, χ_b. This is done by expressing all results in terms of the effective interaction parameter,

$$\chi = \left(1 - \frac{6\alpha}{\pi^2} l\Lambda\right)\chi_b, \tag{37}$$

where $\alpha = 1.221\,375$ for cubic grids,[61,68] $l \equiv 1/\rho_0 a^2$ is the packing length, and $\Lambda \equiv \pi/\Delta$ is a wavevector cutoff. Grywacz *et al.*[122] have since provided more rigorous evidence that the theory is indeed renormalizable.

Although the simple linear renormalization in Eq. (37) works well in FTS for large $\bar{N}$,[61] it fails for realistic values of $\bar{N}$.[62] Beardsley and Matsen[63] recently resolved the problem by instead defining χ using the Morse calibration developed for particle-based simulations.[70] In this approach, the FTS are performed for a fixed relative grid spacing, Δ/a, and relative segment density, $\rho_0 a^3$, where N defines the number of numerical integration steps along the polymer contour such that a corresponds to the typical distance the chain "diffuses" in each step. The calibration is then performed by fitting the peak of the structure function, $S(k^*)$, from the FTS to that of ROL, assuming the nonlinear relationship

$$\chi = \frac{z_\infty \chi_b + c_1 \chi_b^2}{1 + c_2 \chi_b}, \tag{38}$$

where c_1 and c_2 are the fitting parameters. The parameter z_∞ is set to the relative number of intermolecular contacts in an athermal melt (i.e., $\chi_b = 0$), which ensures that mean field theory is recovered at large $\bar{N}$. Provided that $a \lesssim \Delta$, one can show that

$$z_\infty = 1 - \frac{6\alpha}{\pi^2} l\Lambda, \tag{39}$$

which implies that the Morse calibration reduces to the renormalization in Eq. (37) at large $\bar{N}$.

The calibration has been demonstrated for L-FTS with $\Delta = a$ and $\rho_0 = 8/a^3$, which gave coefficients of $z_\infty = 0.7084$, $c_1 = 1.246$, and $c_2 = 1.367$.[68] Figure 5 illustrates the quality of the fit for $S(k^*)$, and

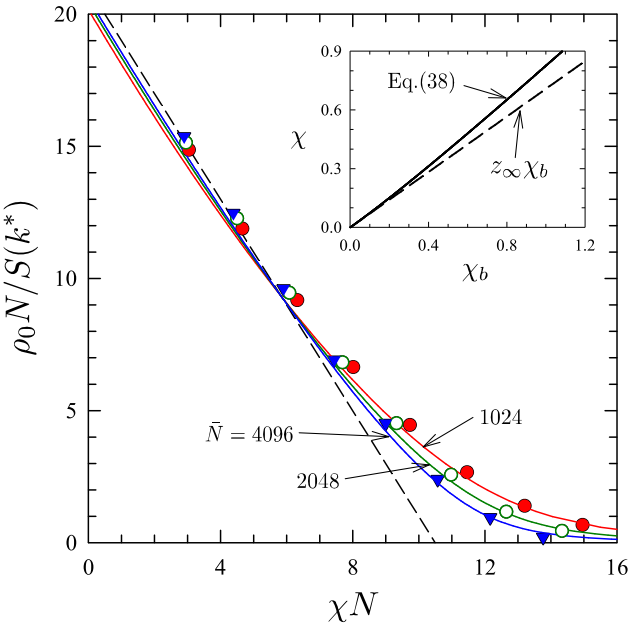

FIG. 5. Inverse peak height of the structure function, $S^{-1}(k^*)$, from L-FTS performed with $\Delta = a$ and $\rho_0 = 8/a^3$, plotted in terms of the effective χ parameter and the invariant polymerization index, $\bar{N} = 64N$. Solid curves denote ROL predictions, and the dashed curve is the RPA prediction. The inset compares the nonlinear relationship between χ and χ_b, Eq. (38), with the linear approximation, $\chi \approx z_\infty \chi_b$, Eq. (37).

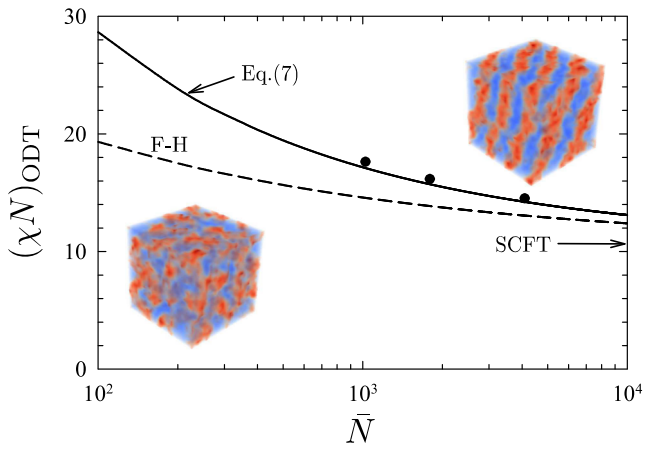

FIG. 6. ODTs from L-FTS plotted in terms of the effective χ and invariant polymerization index, $\bar{N}$. The dashed curve denotes the Fredrickson–Helfand prediction from Eq. (1),[50] and the solid curve shows the universal prediction from Eq. (7).[10]

the inset shows the resulting relationship between the bare χ_b and the effective χ. As a consequence of the partial saddle-point approximation, the L-FTS prediction for $S(k^*)$ (symbols) is unable to capture the deviation of ROL (solid curves) from RPA (dashed curve) at low segregations. This could potentially be remedied by performing CL-FTS, but nevertheless, the inaccuracy is not terribly large for $\bar{N} \gtrsim 10^3$. Using this calibration, the ODTs for diblocks of lengths $N = 16$, 28, and 64 are plotted in Fig. 6 in terms of χ and $\bar{N}$. As required, they compare well with the universal curve, Eq. (7), but there is, nevertheless, a slight deviation that emerges for the shorter polymers. This could be due to the inaccuracy of the partial saddle-point approximation, but it could also be due to a breakdown in universality, which will ultimately occur if the number of integration steps, N, becomes too small.

An alternative strategy is to remove the UV divergence by modifying the standard GCM so as to avoid either zero-range interactions, 1D polymers, or strict incompressibility.[70] This is, in fact, what Delaney and Fredrickson[56] did by introducing compressibility and smearing the interactions.[54,55] However, this alters the model, and thus, the results no longer pertain to the standard GCM. As with any other model, it needs to be mapped back onto the standard GCM. One issue, however, is the range of the interactions. If the range is too large compared to the relevant coarse-grained length scales (e.g., the width of the internal interfaces), then the simulations will not conform to the universal behavior that we are generally interested in.

X. GENERALIZATION OF SCFT AND FTS

One of the main strengths of the field theoretic approach is its incredible diversity. In particular, it is capable of handling complicated polymeric architectures with a minimal increase in computational effort relative to that of the simple diblock,[66,131] which is certainly not the case for traditional particle-based simulations. Furthermore, it can be adapted to a variety of ensembles,[67,132,133] which is hugely advantageous when dealing with blends. For the case of AB-type systems, the only required modification is to the

Hamiltonian, $H_Q[W_-, W_+]$, for non-interacting polymers in the fields $W_-(\mathbf{r})$ and $W_+(\mathbf{r})$. The expression in Eq. (15) for n non-interacting diblocks in a canonical ensemble is simply replaced with the corresponding expression for the system of interest in the ensemble of interest. Of course, this also involves changes to Eqs. (24) and (25) for the composition, $\phi_-(\mathbf{r})$, and total concentration, $\phi_+(\mathbf{r})$, respectively, but that is also straightforward. The extension to three or more chemically distinct components (e.g., ABC-type systems) is somewhat more involved.[128] In particular, it introduces additional fields, which may be real- or imaginary-valued depending on the interaction parameters. This is no problem for CL-FTS, but it remains to be seen if L-FTS also work when the saddle-point approximation is applied to multiple fields.

Universality will ultimately break down at low molecular weights, and at that point, additional features omitted by the standard GCM will start to become relevant. Although quantitative predictions are no longer possible, the field theoretic approach can still be modified in order to study the qualitative effects. For instance, it is straightforward to include compressibility or a finite range to the interactions.[17,56] One can also swap the Gaussian chains for other polymeric models, such as worm-like chains with a fixed contour length and an adjustable flexibility.[134–136] This particular model is well suited for situations where the stiffness, finite extensibility, and/or bond orientation of the polymers become important.[137–139] The worm-like chain also possesses the nice property that it reduces to a Gaussian chain in the limit of infinite flexibility.[140] The only problem, though, is that the corresponding partial partition functions, $q(\mathbf{r}, \mathbf{u}, s)$ and $q^\dagger(\mathbf{r}, \mathbf{u}, s)$, satisfy a more complicated diffusion equation involving the chain position, $\mathbf{r}$, and orientation, $\mathbf{u}$. This complication hinders its application in SCFT[141,142] and prevents any reasonable hope for FTS. A simpler alternative is the freely-jointed chain, consisting of N point-like beads connected by bonds of arbitrary potential.[72,143,144] Although there is no bending energy, the bonds can still accommodate a finite extensibility. In the case of this model, however, the numerics of SCFT and FTS remain virtually the same as for the continuous Gaussian chain.

XI. NUMERICAL METHODS

The importance of numerical methods cannot be overstated. Although SCFT was introduced to the block polymer field in 1975,[17] it took two decades for it to gain traction. Naturally, the increase in computational power was important, but equally so was the development of computational techniques. The two main challenges were solving the diffusion equation and locating the saddle points.

With regard to the diffusion equation, the two leading methods are the spectral algorithm, which expands spatially dependent quantities in terms of M symmetrized basis functions,[26] and the pseudospectral algorithm, which expands in terms of M plane waves.[91] The computational cost of the spectral and pseudospectral methods scales as M^3 and $M \ln M$, respectively, which implies that the former is best at weaker segregations, while the latter is best at stronger segregations.

The saddle points are determined by iterative methods of which the three leading ones are the Broyden algorithm,[38] Anderson mixing (AM),[38,145,146] and a semi-implicit-Seidel (SIS) scheme.[147] The Broyden algorithm typically converges in just a few iterations, but the first iteration requires the costly evaluation of a Jacobian. The latter two are Jacobian-free methods, but they take on the order of 100 iterations to achieve satisfactory accuracy. In general, they are best when $M \gtrsim 100$. Based on the few documented illustrations of AM[38,145] and SIS,[110,147] the AM iterations seem to perform somewhat better. Furthermore, they take about half the time to execute because they only require one rather than two evaluations of $q(\mathbf{r}, s)$ and $q^\dagger(\mathbf{r}, s)$. AM can also optimize the unit cell dimensions in parallel with solving the field equations,[148] although this is likely possible with SIS too.

The only reliable way to determine the best algorithm is to perform direct head-to-head comparisons. AM and SIS have yet to be compared, but the spectral and pseudospectral methods have.[38] Naturally, the comparison should be performed under typical conditions using optimized code. In the case of the spectral method, a considerable amount of the cost is associated with the diagonalization of $M \times M$ matrices, but there are still significant efficiencies to be had regarding how, for example, matrix multiplications are handled. The computational cost of the pseudospectral method is 90% dominated by fast Fourier transforms,[145] and thus the implementation is relatively insensitive to the other details. Nevertheless, there are simple variations that can greatly improve the efficiency, in particular, the inclusion of Richardson extrapolation.[103]

For the SCFT phase diagrams in Fig. 1 as well as similar ones involving more complicated architectures,[143] the spectral method has proven best. It generally requires $M \lesssim 100$ for the classical phases, which can be solved in a fraction of a second on a single CPU. Although M approaches 1000 for complex phases, the computational time still remains less than 10 min. Not until the segregation reaches $\chi N \approx 50$ does the pseudospectral algorithm start to overtake the spectral algorithm. Naturally, these speeds can all be improved with parallel computing, such as calculating $q(\mathbf{r}, t)$ and $q^\dagger(\mathbf{r}, t)$ simultaneously. Opportunities for further reductions in time are also possible with GPUs.[149,150] Nevertheless, as it stands, the computational time of either method is relatively modest and so other considerations become relevant. The spectral method benefits from the fact that the numerical inaccuracy is easier to manage because the only source is the truncation of basis functions. On the other hand, the pseudospectral algorithm is simpler to implement due to the fact that it avoids the use of symmetrized basis functions. Perhaps, a more significant consideration is the fact that the pseudospectral algorithm for SCFT is easily converted to FTS.[68,72]

The composition fluctuations in FTS break the symmetry of the ordered phases, and so the pseudospectral algorithm becomes the natural choice. Although Richardson extrapolation can greatly increase the computational efficiency by reducing the required number of integration steps along the polymer contour, this improvement requires sufficiently smooth fields. Thus, it will not necessarily benefit FTS. Audus *et al.*[55] have indeed concluded that the pseudospectral method is marginally better without Richardson extrapolation, although Beardsley[152] found a marginal benefit of including Richardson extrapolation; the difference may have something to do with the fact that one comparison was for CL-FTS, while the other was for L-FTS. Nevertheless, there is an alternative to demanding convergence with respect to integration along the chain contour.

In FTS, one can regard the algorithm used to solve the diffusion equation as part of the model.[63] For instance, the basic pseudospectral algorithm corresponds to a polymer chain with N point-like beads connected by harmonic springs of natural length a.[143,144]

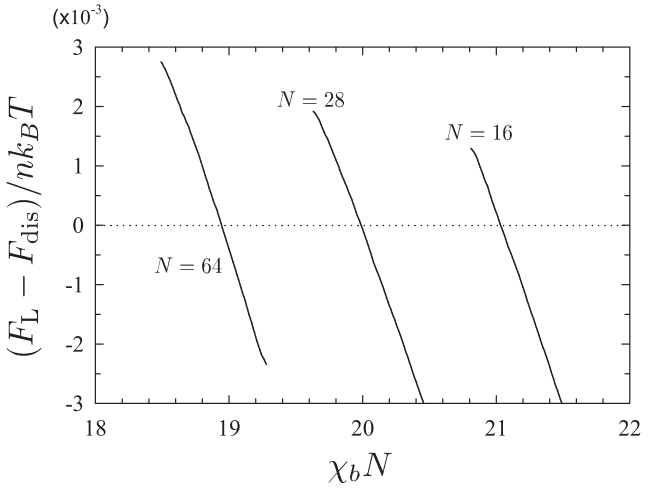

FIG. 7. Free energy difference between the lamellar and disordered phases as a function of the bare χ_b parameter obtained with thermodynamic integration using L-FTS. The resulting ODTs are plotted in Fig. 6.

Likewise, the pseudospectral algorithm with Richardson extrapolation can be regarded as another model, albeit with a less obvious interpretation. In either case, the FTS is performed with a fixed resolution, Δ/a, and segment density, $\rho_0 a^3$. To compensate for the finite step size along the chain contour, the χ_b of the FTS is mapped onto the χ of the standard GCM using the Morse calibration. Beardsley and Matsen[68] initially demonstrated that this approach works well with Richardson extrapolation, but Beardsley[152] has since found that it also works similarly well with the basic algorithm. Although the latter requires a larger N to maintain universality, this is facilitated by the computational savings of removing Richardson extrapolation. In light of this fact, we recommend the basic algorithm for the esthetic reason that it equates to a standard bead-spring model.

As always, the free energy cannot be obtained directly from simulations, but it is possible to evaluate derivatives of the free energy that can be integrated to obtain changes in free energy, provided that the integration does not cross a phase transition.[151] It was with thermodynamic integration that Lennon *et al.*[53] calculated their ODTs for diblock polymer melts. They did this by creating a composite Hamiltonian that bridged between an Einstein crystal of independent harmonic oscillators, for which the free energy is known, and the polymeric system. Once the free energy of the polymeric system was obtained for the disordered and ordered phases, they evaluated the change in free energy with respect to χ. Figure 7 shows an analogous calculation for symmetric diblocks using L-FTS.[68] This particular implementation uses continuous integration, whereby the ensemble average of the free energy derivatives and the integration are evaluated simultaneously.[153,154] The resulting ODTs are the same ones plotted in Fig. 6.

Thermodynamic integration is a versatile method with considerable scope for future developments. For example, instead of using the Einstein crystal as a reference for calibrating the absolute free energy, it might be possible to integrate from the known free energy of the SCFT solution using $\bar{N}$ as the integrating variable. There is also a Gibbs–Duhem scheme for tracing out first-order phase boundaries.[155] Thermodynamic integration may also allow for on-the-fly optimization of unit cell dimensions, which still remains an outstanding issue for triply periodic phases.[56,62]

XII. DISCUSSION AND FUTURE OUTLOOK

The standard Gaussian chain model (GCM), underpinning SCFT and FTS, plays the role of a "meter stick" with which all systems, experimental and computational, are measured. As we have stressed, the ability to accurately map other systems onto the standard GCM relies on universality. One needs to remember, though, that universality only applies when the assumptions of the standard GCM are satisfied. For instance, the persistence length of the polymer needs to be short relative to the length of any block, and the interactions must be short range relative to all the coarse-grained length scales (e.g., the width of the internal interfaces). Universality will ultimately break down if N becomes too small. The point at which this happens will differ for different models, in particular, it will happen sooner for stiffer molecules.[156] Once it does break down, the behavior will start to depend on additional quantities, such as the stiffness and the end-groups of the polymers.[157–159] Furthermore, it will no longer be possible to characterize the molecular interactions by a single χ parameter.[160] Nevertheless, the breakdown will not occur abruptly, and so the GCM may still remain semi-quantitative.

It is worth noting that the field theoretic approach does not prevent chain crossings. While this constraint is important in polymer dynamics, it does not generally impact equilibrium behavior. The one exception, however, is when the polymeric architecture involves a closed loop, such as for cyclic or ring diblock polymers.[161–164] In this case, the constraint limits the number of accessible configurations. If the system starts off with unknotted and unconcatenated polymers, the constraint will ensure that they remain so. In simple homopolymer melts, this results in compact polymer configurations (i.e., $R_g \propto N^{1/3}$),[165] an effect which the field theoretic approach is incapable of capturing.

The SCFT of the standard GCM has matured to the point where the calculation of phase diagrams, such as those in Fig. 1, requires no more than a day of CPU time on a desktop computer. Nevertheless, further computational efficiencies will always be welcome. They could greatly benefit the development of strategies for discovering new candidate phases[90–95] or tackling the inverse problem.[96,97] With sufficiently fast and stable algorithms, it may become possible to automate the procedure for calculating phase diagrams, perhaps with the aid of machine learning.

While algorithms for the Gaussian chain are remarkably fast, this is certainly not the case for the worm-like chain.[134–136] Jiang and Chen[142] managed to calculate diblock phase diagrams at modest degrees of segregation, but the numerical accuracy was visibly compromised by the high computational costs. There have been some significant advances recently,[166,167] but further developments would be particularly valuable. They would, among other things, enhance our ability to investigate the effects of finite flexibility, finite extensibility, and/or bond orientation,[137–139] all of which become relevant for lower molecular-weight systems.

In contrast to SCFT, FTS are relatively new and very much in the development stage. The challenge is to achieve quantitative results for experimentally relevant conditions. This not only requires

algorithms that can cope with realistic invariant polymerizations, $\bar{N}$, but also a way of dealing with the UV divergence. This has just recently been accomplished by combining the partial saddle-point approximation, Langevin simulations, and the Morse calibration.[68] Now that the major obstacles have been overcome, FTS are likely to gain widespread use. The fact that the algorithm is so similar to that of SCFT will certainly help.

Past studies[57,58] have found the partial saddle-point approximation to be accurate, but it will become less so as $\bar{N}$ is reduced. The clearest evidence for this is the inability to capture the departure of $S(k^*)$ from the RPA prediction at small χN, as shown in Fig. 5. Although the inaccuracy still appears to be relatively minor for $\bar{N} \gtrsim 10^3$, it should, nevertheless, be examined more thoroughly at some point. Of course, it would be preferable to perform FTS with fully fluctuating fields, and there are, in fact, some systems for which it is essential to treat incompressibility rigorously, such as block polymer nanocomposites.[54,133,168] Some researchers[169,170] have pointed out unphysical behavior in SCFT calculations,[171,172] whereby polymers penetrate the interior of nanoparticles. This would also be a problem in L-FTS.

Although CL-FTS offer a way of strictly enforcing incompressibility, they suffer from an instability, which becomes increasingly serious as $\bar{N}$ is reduced.[54,55] While ordinary Langevin simulations always produce stable trajectories that gravitate toward equilibrium, this is not necessarily the case for complex Langevin simulations. If the trajectories are stable, they will tend toward equilibrium,[173,174] but stability is not guaranteed.[73] Koski and Riggleman[54] managed to tame the instability by introducing compressibility into their nanocomposite simulations, but too much compressibility could defeat the purpose of using fully fluctuating fields.

Delaney and Fredrickson[56] go further and smear all the interactions in their calculations of the diblock phase diagram. However, their fluctuation correction at $\bar{N} \approx 10^4$ destroys the Fddd phase while still remaining insufficient to produce direct G-to-disorder transitions. Although their results still require a proper calibration of the χ parameter, this will not fix the topology of the phase diagram. The inconsistency with experiments is likely due to excessive smearing of the interactions, resulting in a breakdown of universality. It might be useful to investigate the instability in CL-FTS in order to find a milder modification to remove the UV divergence. One should also remain openminded about alternative ways of performing the statistical mechanics, even if they are somewhat more computational.[52]

On this front, Fredrickson and co-workers[175,176] are exploring an entirely different approach, the "coherent states" formulation of polymer field theory originally proposed by Edwards and Freed.[177] In the current "auxiliary field" formalism, the partial partition functions, $q(\mathbf{r}, t)$ and $q^\dagger(\mathbf{r}, t)$, are calculated by solving the diffusion equation and as such are explicitly dependent on the fields, $W_-(\mathbf{r})$ and $W_+(\mathbf{r})$. In the coherent states framework, $q(\mathbf{r}, t)$ and $q^\dagger(\mathbf{r}, t)$ are independent dynamical variables of the corresponding Hamiltonian, $H_{CS}[W_-, W_+, q, q^\dagger]$. The statistical mechanics of H_{CS} can again be solved using the saddle-point approximation, leading to the same SCFT solution, or it can be performed with FTS. At the moment, the FTS are not particularly efficient,[175] but the SCFT appears to be competitive.[176] It is still early days, and we will have to wait to see what develops.

Without question, the field theoretic approach is here to stay. SCFT is a highly, if not the most, successful theory in the field of soft condensed matter. Its success in predicting the relative stability of the complex phases (e.g., G, D, PL, and Fddd) as well as the different spherical phases (e.g., S, S_{cp}, σ, and A15) is an impressive testament to its performance, and there are numerous other systems for which it has performed similarly. However, SCFT still fails to treat disordered-type morphologies accurately, which is the prime motivation for developing FTS. This is particularly important in some systems, such as ternary diblock–homopolymer blends[57,60,67] and miktoarm starblock melts,[131] where fluctuations are known to have profound qualitative effects on the phase behavior.

Now that FTS are able to handle experimentally relevant conditions, they are likely to gain widespread use. Naturally, many researchers will want to concentrate on applications of FTS, but it is also important to continue with development and testing. As history has demonstrated, there are great benefits to be had from improving the numerical algorithms. In doing so, new innovations will have to be given the opportunity to develop, but also the ineffective algorithms will need to be weeded out. This should be done carefully based on detailed head-to-head comparisons rather than speculative arguments. Given the current state-of-the-art and the opportunities for further improvements, the field theoretic approach is likely to dominate the field of block polymers for the foreseeable future.

ACKNOWLEDGMENTS

My research in SCFT and FTS was made possible thanks to the dedicated work of my postdocs, in particular, Tom Beardsley, Jaeup Kim, Russell Spencer, Pawel Stasiak, Russell Thompson, and Bart Vorselaars. I have also benefited from valuable discussions with Frank Bates, Kari Dalnoki-Veress, Glenn Fredrickson, Damian Hajduk, Ian Hamley, Marc Hillmyer, Dave Morse, Marcus Müller, Tony Ryan, Friederike Schmid, and An-Chang Shi.

REFERENCES

[1] I. W. Hamley, *The Physics of Block Copolymers* (Oxford University Press, Oxford, 1998).
[2] F. S. Bates and G. H. Fredrickson, Phys. Today **52**(2), 32 (1999).
[3] F. S. Bates, M. A. Hillmyer, T. P. Lodge, C. M. Bates, K. T. Delaney, and G. H. Fredrickson, Science **336**, 434 (2012).
[4] G. Polymeropoulos, G. Zapsas, K. Ntetsikas, P. Bilalis, Y. Gnanou, and N. Hadjichristidis, Macromolecules **50**, 1253 (2017).
[5] H. Feng, X. Lu, W. Wang, N.-G. Kang, and J. W. Mays, Polymers **9**, 494 (2017).
[6] C. M. Bates and F. S. Bates, Macromolecules **50**, 3 (2017).
[7] J. Glaser, J. Qin, P. Medapuram, M. Müller, and D. C. Morse, Soft Matter **8**, 11310 (2012).
[8] J. Glaser, P. Medapuram, and D. C. Morse, Macromolecules **47**, 851 (2014).
[9] F. S. Bates, M. F. Schulz, A. K. Khandpur, S. Förster, and J. H. Rosedale, Faraday Discuss. **98**, 7 (1994).
[10] J. Glaser, P. Medapuram, T. M. Beardsley, M. W. Matsen, and D. C. Morse, Phys. Rev. Lett. **113**, 068302 (2014).
[11] P. Medapuram, J. Glaser, and D. C. Morse, Macromolecules **48**, 819 (2015).
[12] J. D. Willis, T. M. Beardsley, and M. W. Matsen, J. Chem. Phys. **150**, 204906 (2019).
[13] T. Ghasimakbari and D. C. Morse, Macromolecules **51**, 2335 (2018).
[14] T. M. Beardsley and M. W. Matsen, Phys. Rev. Lett. **117**, 217801 (2016).
[15] M. W. Matsen, J. Phys.: Condens. Matter **14**, R21 (2002).

[16]S. F. Edwards, Proc. Phys. Soc. London **85**, 613 (1965).
[17]E. Helfand, J. Chem. Phys. **62**, 999 (1975).
[18]L. Leibler, Macromolecules **13**, 1602 (1980).
[19]A. N. Semenov, Sov. Phys. JETP **61**, 733 (1985).
[20]E. Helfand and Z. R. Wasserman, in *Development in Block Copolymers*, edited by I. Goodman (Elsevier, New York, 1982).
[21]J. D. Vavasour and M. D. Whitmore, Macromolecules **25**, 5477 (1992).
[22]E. L. Thomas, D. B. Alward, D. J. Kinning, D. C. Martin, D. L. Handlin, and L. J. Fetters, Macromolecules **19**, 2197 (1986).
[23]D. A. Hajduk, P. E. Harper, S. M. Gruner, C. C. Honeker, G. Kim, and E. L. Thomas, Macromolecules **27**, 4063 (1994).
[24]M. F. Schulz, F. S. Bates, K. Almdal, and K. Mortensen, Phys. Rev. Lett. **73**, 86 (1994).
[25]I. W. Hamley, K. A. Koppi, J. H. Rosedale, F. S. Bates, K. Almdal, and K. Mortensen, Macromolecules **26**, 5959 (1993).
[26]M. W. Matsen and M. Schick, Phys. Rev. Lett. **72**, 2660 (1994).
[27]D. A. Hajduk, P. E. Harper, S. M. Gruner, C. C. Honeker, G. Kim, E. L. Thomas, and L. J. Fetters, Macromolecules **28**, 2570 (1995).
[28]D. A. Hajduk, H. Takenouchi, M. A. Hillmyer, F. S. Bates, M. E. Vigild, and K. Almdal, Macromolecules **30**, 3788 (1997).
[29]M. E. Vigild, K. Almdal, K. Mortensen, I. W. Hamley, J. P. A. Fairclough, and A. J. Ryan, Macromolecules **31**, 5702 (1998).
[30]X. Cheng, L. Lin, W. E, P. Zhang, and A.-C. Shi, Phys. Rev. Lett. **104**, 148301 (2010).
[31]C. Yeung, A.-C. Shi, J. Noolandi, and R. C. Desai, Macromol. Theory Simul. **5**, 291 (1996).
[32]T. M. Beardsley and M. W. Matsen, Eur. Phys. J. E **32**, 255 (2010).
[33]C. A. Tyler and D. C. Morse, Phys. Rev. Lett. **94**, 208302 (2005).
[34]M. Takenaka, T. Wakada, S. Akasaka, S. Nishitsuji, K. Saijo, H. Shimizu, M. I. Kim, and H. Hasegawa, Macromolecules **40**, 4399 (2007).
[35]Y.-C. Wang, K. Matsuda, M. I. Kim, A. Miyoshi, S. Akasaka, S. Nishitsuji, K. Saijo, H. Hasegawa, K. Ito, T. Hikima, and M. Takenaka, Macromolecules **48**, 2211 (2015).
[36]S. Lee, C. Leighton, and F. S. Bates, Proc. Natl. Acad. Sci. U. S. A. **111**, 17723 (2014).
[37]A. N. Semenov, Macromolecules **22**, 2849 (1989).
[38]M. W. Matsen, Eur. Phys. J. E **30**, 361 (2009).
[39]M. W. Matsen and F. S. Bates, Macromolecules **29**, 1091 (1996).
[40]N. Sakamoto and T. Hashimoto, Macromolecules **31**, 8493 (1998).
[41]C. D. Han, N. Y. Vaidya, D. Kim, G. Shin, D. Yamaguchi, and T. Hashimoto, Macromolecules **33**, 3767 (2000).
[42]S. Lee, M. J. Bluemle, and F. S. Bates, Science **330**, 349 (2010).
[43]N. Xie, W. Li, F. Qiu, and A.-C. Shi, ACS Macro Lett. **3**, 906 (2014).
[44]M. W. Schulze, R. M. Lewise III, J. H. Lettow, R. J. Hickey, T. M. Gillard, M. A. Hillmyer, and F. S. Bates, Phys. Rev. Lett. **118**, 207801 (2017).
[45]R. M. Lewis III, A. Arora, H. K. Beech, B. Lee, A. P. Lindsay, T. P. Lodge, K. D. Dorfman, and F. S. Bates, Phys. Rev. Lett. **121**, 208002 (2018).
[46]A.-C. Shi, private communication (2019).
[47]M. W. Bates, J. Lequieu, S. M. Barbon, R. M. Lewis III, K. T. Delaney, A. Anastaski, C. J. Hawker, G. H. Fredrickson, and C. M. Bates, Proc. Natl. Acad. Sci. U. S. A. **116**, 13194 (2019).
[48]M. Yadav, F. S. Bates, and D. C. Morse, Phys. Rev. Lett. **121**, 127802 (2018).
[49]K. Almdal, J. H. Rosedale, F. S. Bates, G. D. Wignall, and G. H. Fredrickson, Phys. Rev. Lett. **65**, 1112 (1990).
[50]G. H. Fredrickson and E. Helfand, J. Chem. Phys. **87**, 697 (1987).
[51]A. M. Mayes and M. O. de la Cruz, J. Chem. Phys. **95**, 4670 (1991).
[52]V. Ganesan and G. H. Fredrickson, Europhys. Lett. **55**, 814 (2001).
[53]E. M. Lennon, K. Katsov, and G. H. Fredrickson, Phys. Rev. Lett. **101**, 138302 (2008).
[54]J. Koski, H. Chao, and R. A. Riggleman, J. Chem. Phys. **139**, 244911 (2013).
[55]D. J. Audus, K. T. Delaney, H. D. Ceniceros, and G. H. Fredrickson, Macromolecules **46**, 8383 (2013).
[56]K. T. Delaney and G. H. Fredrickson, J. Phys. Chem. B **120**, 7615 (2016).
[57]D. Düchs, V. Ganesan, G. H. Fredrickson, and F. Schmid, Macromolecules **36**, 9237 (2003).
[58]A. Alexander-Katz and G. H. Fredrickson, Macromolecules **40**, 4075 (2007).
[59]E. Reister, M. Müller, and K. Binder, Phys. Rev. **64**, 041804 (2001).
[60]D. Düchs and F. Schmid, J. Chem. Phys. **121**, 2798 (2004).
[61]P. Stasiak and M. W. Matsen, Macromolecules **46**, 8037 (2013).
[62]B. Vorselaars, P. Stasiak, and M. W. Matsen, Macromolecules **46**, 9071 (2015).
[63]T. M. Beardsley and M. W. Matsen, J. Chem. Phys. **150**, 174902 (2019).
[64]R. K. W. Spencer and M. W. Matsen, Macromolecules **49**, 6116 (2016).
[65]R. K. W. Spencer and M. W. Matsen, Macromolecules **51**, 4747 (2018).
[66]R. K. W. Spencer and M. W. Matsen, J. Chem. Phys. **149**, 184901 (2018).
[67]R. K. W. Spencer and M. W. Matsen, J. Chem. Phys. **148**, 204907 (2018).
[68]T. M. Beardsley and M. W. Matsen, Macromolecules **52**, 8840 (2019).
[69]M. O. de la Cruz, S. F. Edwards, and I. C. Sanchez, J. Chem. Phys. **89**, 1704 (1988).
[70]J. Qin and D. C. Morse, J. Chem. Phys. **130**, 224902 (2009).
[71]F. Schmid, J. Phys.: Condens. Matter **10**, 8105 (1998).
[72]G. H. Fredrickson, *The Equilibrium Theory of Inhomogeneous Polymers* (Oxford University Press, New York, 2006).
[73]G. H. Fredrickson, V. Ganesan, and F. Drolet, Macromolecules **35**, 16 (2002).
[74]M. Müller and F. Schmid, in *Advanced Computer Simulation Approaches for Soft Matter Sciences II*, edited by C. Holm and K. Binder (Springer-Verlag, Berlin, 2005).
[75]G. H. Fredrickson, Soft Matter **3**, 1329 (2007).
[76]T. P. Russell, R. P. Hjelm, Jr., and P. A. Seeger, Macromolecules **23**, 890 (1990).
[77]T. Koch and G. R. Strobl, J. Polym. Sci., Part B: Polym. Phys. **28**, 343 (1990).
[78]K. H. Dai and E. J. Kramer, Polymer **35**, 157 (1994).
[79]C. J. Clarke, A. Eisenberg, J. La Scala, M. H. Rafailovich, J. Sokolov, Z. Li, S. Qu, D. Nguyen, S. A. Schwarz, Y. Strzhemechny, and B. B. Sauer, Macromolecules **30**, 4184 (1997).
[80]W. W. Maurer, F. S. Bates, T. P. Lodge, K. Almdal, K. Mortensen, and G. H. Fredrickson, J. Chem. Phys. **108**, 2989 (1998).
[81]W. Zha, C. D. Han, D. H. Lee, S. H. Han, J. K. Kim, J. H. Kang, and C. Park, Macromolecules **40**, 2109 (2007).
[82]S. H. Han and J. Kon Kim, React. Funct. Polym. **69**, 493 (2009).
[83]D. P. Sweat, M. Kim, S. R. Larson, J. W. Choi, Y. Choo, C. O. Osuji, and P. Gopalan, Macromolecules **47**, 6687 (2014).
[84]A. H. Hofman, G. O. R. A. van Ekenstein, A. J. J. Woortman, G. ten Brinke, and K. Loos, Polym. Chem. **6**, 7015 (2015).
[85]G. Miqueland-Garnier and S. Roland, Eur. Polym. J. **84**, 111 (2016).
[86]S. X. Zhou, D. W. Janes, C. B. Kim, C. G. Willson, and C. J. Ellison, Macromolecules **49**, 8332 (2016).
[87]A. B. Burns, D. Christie, W. D. Mulhearn, and R. A. Register, J. Polym. Sci., Part B **57**, 932 (2019).
[88]M. Doi and S. F. Edwards, *The Theory of Polymer Dynamics* (Oxford University Press, Oxford, 1986).
[89]T. S. Bailey, C. M. Hardy, T. H. Epps, and F. S. Bates, Macromolecules **35**, 7007 (2002).
[90]F. Drolet and G. H. Fredrickson, Phys. Rev. Lett. **83**, 4317 (1999).
[91]K. O. Rasmussen and G. Kalosakas, J. Polym. Sci., Part B **40**, 1777 (2002).
[92]Z. Guo, G. Zhang, F. Qiu, H. Zhang, Y. Yang, and A.-C. Shi, Phys. Rev. Lett. **101**, 028301 (2008).
[93]Y. Bohbot-Raviv and Z.-G. Wang, Phys. Rev. Lett. **85**, 3428 (2000).
[94]W. Xu, K. Jiang, P. Zhang, and A.-C. Shi, J. Phys. Chem. B **117**, 5296 (2013).
[95]C. L. Tsai, K. T. Delaney, and G. H. Fredrickson, Macromolecules **49**, 6558 (2016).
[96]S. P. Paradiso, K. T. Delaney, and G. H. Fredrickson, ACS Macro Lett. **5**, 972 (2016).
[97]M. R. Khadilkar, S. P. Paradiso, K. T. Delaney, and G. H. Fredrickson, Macromolecules **50**, 6702 (2017).
[98]M. W. Matsen and F. S. Bates, J. Chem. Phys. **106**, 2436 (1997).

[99]R. K. W. Spencer and M. W. Matsen, Macromolecules **50**, 1681 (2017).
[100]A.-C. Shi, J. Noolandi, and R. Desai, Macromolecules **29**, 6487 (1996).
[101]M. Laradji, A.-C. Shi, R. Desai, and J. Noolandi, Phys. Rev. Lett. **78**, 2577 (1997).
[102]M. W. Matsen, Phys. Rev. Lett. **80**, 4470 (1998).
[103]A. Ranjan, J. Qin, and D. C. Morse, Macromolecules **41**, 942 (2008).
[104]S. T. Milner, T. A. Witten, and M. E. Cates, Macromolecules **21**, 2610 (1988).
[105]P. D. Olmsted and S. T. Milner, Phys. Rev. Lett. **72**, 936 (1994).
[106]P. D. Olmsted and S. T. Milner, Phys. Rev. Lett. **74**, 829 (1995).
[107]P. D. Olmsted and S. T. Milner, Macromolecules **31**, 4011 (1998).
[108]A. E. Likhtman and A. N. Semenov, Macromolecules **27**, 3103 (1994).
[109]A. E. Likhtman and A. N. Semenov, Macromolecules **30**, 7273 (1997).
[110]E. W. Cochran, C. J. Garcia-Cervera, and G. H. Fredrickson, Macromolecules **39**, 2449 (2006).
[111]M. W. Matsen, J. Chem. Phys. **114**, 10528 (2001).
[112]A. E. Likhtman and A. N. Semenov, Europhys. Lett. **51**, 307 (2000).
[113]M. W. Matsen, J. Chem. Phys. **121**, 1938 (2004).
[114]M. W. Matsen, Eur. Phys. J. E **33**, 297 (2010).
[115]M. W. Matsen, J. Chem. Phys. **106**, 7781 (1997).
[116]M. W. Matsen and F. S. Bates, Macromolecules **29**, 7641 (1996).
[117]V. E. Podneks and I. W. Hamley, JETP Lett. **64**, 617 (1996).
[118]S. T. Milner and P. D. Olmsted, J. Phys. II **7**, 249 (1997).
[119]A. Ranjan and D. C. Morse, Phys. Rev. E **74**, 011803 (2006).
[120]B. Miao and R. A. Wickham, J. Chem. Phys. **128**, 054902 (2008).
[121]F. S. Bates, J. H. Rosedale, G. H. Fredrickson, and C. J. Glinka, Phys. Rev. Lett. **61**, 2229 (1988).
[122]P. Grzywacz, J. Qin, and D. C. Morse, Phys. Rev. E **76**, 061802 (2007).
[123]J. Qin, P. Grzywacs, and D. C. Morse, J. Chem. Phys. **135**, 084902 (2011).
[124]J. Qin and D. C. Morse, Phys. Rev. Lett. **108**, 238301 (2012).
[125]T. Ohta and K. Kawasaki, Macromolecules **19**, 2621 (1986).
[126]M. Muthukumar, Macromolecules **26**, 5259 (1993).
[127]J. V. Liu, C. J. Garcia-Cervera, K. T. Delany, and G. H. Fredrickson, Macromolecules **52**, 2878 (2019).
[128]D. Düchs, K. T. Delaney, and G. H. Fredrickson, J. Chem. Phys. **141**, 174103 (2014).
[129]P. J. Rossky, J. D. Doll, and H. L. Friedman, J. Chem. Phys. **69**, 4628 (1978).
[130]F. A. Detcheverry, D. Q. Pike, P. F. Nealey, M. Müller, and J. J. de Pablo, Phys. Rev. Lett. **102**, 197801 (2009).
[131]Y. X. Liu, K. T. Delaney, and G. H. Fredrickson, Macromolecules **50**, 6263 (2017).
[132]R. A. Riggleman and G. H. Fredrickson, J. Chem. Phys. **132**, 024104 (2010).
[133]J. P. Koski and R. A. Riggleman, J. Chem. Phys. **146**, 164903 (2017).
[134]O. Kratky and G. Porod, Recl. Trav. Chim. Pays-Bas **68**, 1106 (1949).
[135]N. Saito, K. Takahashi, and Y. Yunoki, J. Phys. Soc. Jpn. **22**, 219 (1967).
[136]Y. Jiang, S. Li, and J. Z. Y. Chen, Eur. Phys. J. E **39**, 91 (2016).
[137]G. T. Pickett and T. A. Witten, Macromolecules **25**, 4569 (1992).
[138]J. P. Witter, H. Meyer, J. Baschnagel, A. Johner, S. Obukhov, L. Mattioni, M. Müller, and A. N. Semonov, Phys. Rev. Lett. **93**, 147801 (2004).
[139]J. P. Witter, P. Beckrich, H. Meyer, A. Cavallo, A. Johner, and J. Baschnagel, Phys. Rev. E **76**, 011803 (2007).
[140]D. C. Morse and G. H. Fredrickson, Phys. Rev. Lett. **73**, 3235 (1994).
[141]M. W. Matsen, J. Chem. Phys. **104**, 7758 (1996).
[142]Y. Jiang and J. Z. Y. Chen, Phys. Rev. Lett. **110**, 138305 (2013).
[143]M. W. Matsen, Macromolecules **45**, 8502 (2012).
[144]J. Park, D. Yong, Y. Kim, and J. U. Kim, J. Chem. Phys. **150**, 234901 (2017).
[145]P. Stasiak and M. W. Matsen, Eur. Phys. J. E **34**, 110 (2011).
[146]R. B. Thompson, K. O. Rasmussen, and T. Lookman, J. Chem. Phys. **120**, 31 (2004).
[147]H. D. Ceniceros and G. H. Fredrickson, Multiscale Model. Simul. **2**, 452 (2004).
[148]A. Arora, D. C. Morse, F. S. Bates, and K. D. Dorfman, J. Chem. Phys. **146**, 244902 (2017).
[149]K. T. Delaney and G. H. Fredrickson, Comput. Phys. Commun. **184**, 2102 (2013).
[150]G. K. Cheong, A. Chawla, D. C. Morse, and K. D. Dorfman, Eur. Phys. J. E **43**, 15 (2020).
[151]D. Frenkel and A. J. C. Ladd, J. Chem. Phys. **81**, 3188 (1984).
[152]T. M. Beardsley, private communication (2019).
[153]M. Watanabe and W. P. Reinhardt, Phys. Rev. Lett. **65**, 3301 (1990).
[154]R. K. W. Spencer, B. Vorselaars, and M. W. Matsen, Macromol. Theory Simul. **26**, 1700036 (2017).
[155]D. A. Kofke, Molec. Phys. **78**, 1331 (1993).
[156]S. Mao, Q. MacPherson, and A. J. Spakowitz, Phys. Rev. Lett. **120**, 067802 (2018).
[157]H. Frielinghaus, W. B. Pedersen, P. S. Larsen, K. Almdal, and K. Mortensen, Macromolecules **34**, 1096 (2001).
[158]T. G. Gillard, P. Medapuram, D. C. Morse, and F. S. Bates, Macromolecules **48**, 2801 (2015).
[159]J. Kim, H. Y. Jung, and M. J. Park, Macromolecules **53**, 746 (2020).
[160]C. Sinturel, F. S. Bates, and M. A. Hillmyer, ACS Macro Lett. **4**, 1044 (2015).
[161]H. Iatrou, N. Hadjichristidis, G. Meier, H. Frielinghaus, and M. Monkenbusch, Macromolecules **35**, 5426 (2002).
[162]Y. Zhu, S. P. Gido, H. Iatrou, N. Hadjichristidis, and J. W. Mays, Macromolecules **36**, 148 (2003).
[163]J. E. Poelma, K. Ono, D. Miyajima, T. Aida, K. Satoh, and C. J. Hawker, ACS Nano **6**, 10845 (2012).
[164]T. E. Gartner III, T. Kubo, Y. Seo, M. Tansky, L. M. Hall, B. S. Sumerlin, and T. H. Epps III, Macromolecules **50**, 7169 (2017).
[165]J. D. Halverson, W. B. Lee, G. S. Grest, A. Y. Grosberg, and K. Kremer, J. Chem. Phys. **134**, 204904 (2011).
[166]W. Song, P. Tang, H. Zhang, Y. Yang, and A.-C. Shi, Macromolecules **42**, 6300 (2009).
[167]A. F. Hannon, R. J. Kline, and D. DeLongchamp, J. Polym. Sci., Part B **57**, 29 (2019).
[168]H. Chao, B. A. Hagberg, and R. A. Riggleman, Soft Matter **10**, 8083 (2014).
[169]S. W. Sides, B. J. Kim, E. J. Kramer, and G. H. Fredrickson, Phys. Rev. Lett. **96**, 250601 (2006).
[170]M. W. Matsen and R. B. Thompson, Macromolecules **41**, 1853 (2008).
[171]R. B. Thompson, V. V. Ginzburg, M. W. Matsen, and A. C. Balazs, Science **292**, 2469 (2001).
[172]R. B. Thompson, V. V. Ginzburg, M. W. Matsen, and A. C. Balazs, J. Chem. Phys. **35**, 1060 (2002).
[173]S. Lee, Nucl. Phys. B **413**, 827 (1994).
[174]H. Gausterer, Nucl. Phys. A **642**, c239 (1998).
[175]X. Man, K. T. Delaney, M. C. Villet, H. Orland, and G. H. Fredrickson, J. Chem. Phys. **140**, 024905 (2014).
[176]D. L. Vigil, C. J. Garcia-Cervera, K. T. Delaney, and G. H. Fredrickson, ACS Macro Lett. **8**, 1402 (2019).
[177]S. F. Edwards and K. F. Freed, J. Phys. C: Solid State Phys. **3**, 739 (1970).